Energy-Transfer Sensitization of BODIPY Fluorescence in a Dyad with a Two-Photon Absorbing Antenna Chromophore

Antonio Dominguez-Alfaro,[a] Vânia F. Pais,[a] David B. Guzmán-Ríos,[a] Daniel Collado,[b,c] Francisco Nájera,[b,c] Ezequiel Pérez-Inestrosa,[b,c,*] Uwe Pischel[a,*]

[a] CIQSO – Center for Research in Sustainable Chemistry, University of Huelva, Campus de El Carmen s/n, E-21071 Huelva, Spain.

[b] Departamento de Química Orgánica, Facultad de Ciencias, Universidad de Málaga, E-29071 Málaga, Spain.

[c] Instituto de Investigación Biomédica de Málaga y Plataforma en Nanomedicina – IBIMA, Plataforma Bionand, Parque Tecnológico de Andalucía, E-29590 Málaga, Spain.

* Corresponding authors.

E-mail: inestrosa@uma.es (E.P.-I.), uwe.pischel@diq.uhu.es (U.P.).

Highlights

- A BODIPY-Prodan dyad with a light-harvesting antenna and a non-conjugating linker was synthesized.
- Highly efficient two-photon-induced energy transfer mediates the excited state communication between the two chromophores.
- Intramolecular photoinduced electron transfer is controlled by solvent polarity.
- Two-photon excitation under conditions of the imaging of N13 microglial cells is demonstrated.

Abstract

A bichromophoric dyad composed of a Prodan-derived moiety and a BODIPY dye was prepared, photophysically characterized, and tested for multiphoton fluorescence microscopy of N13 microglial cells. The dyad shows highly efficient energy transfer, independent on the solvent polarity of the medium. However, in polar media photoinduced electron transfer is a competitive pathway. The Prodan-derived chromophore shows significant two-photon absorption. Hence, it can be used a two-photon-absorbing antenna for the sensitization of BODIPY fluorescence.

Graphical abstract

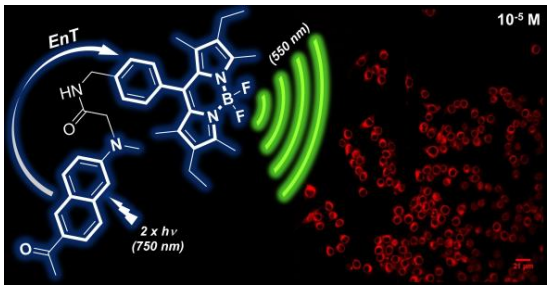

Keywords

BODIPY dyes

Energy transfer

Electron transfer

Two-photon absorption

Bioimaging

1. Introduction

Boron dipyrromethene (BODIPY) compounds are among the archetypal functional dyes in bio-relevant applications and have found widespread use as labels for cell imaging [1–7], temperature or viscosity probes [8–10], chemosensors [11–14], and photosensitizers for singlet oxygen [4,15–19]. The preference as an imaging probe is motivated by the high molar absorption coefficients (*ca*. 60000–80000 $M^{-1}cm^{-1}$), paired with highly efficient fluorescence (emission quantum yields Φ_f *ca*. 0.6–1.0) [17,20–24]. A generally observed drawback of BODIPY dyes is their rather small Stokes shift (*ca*. 500–800 cm^{-1}), which may cause problems such as excitation straylight detection, re-absorption of emitted photons or homo-energy transfer [23–25]. A viable strategy to overcome this shortcoming is the structural integration in antenna-substituted dyad designs that enable the observation of the highly efficient BODIPY fluorescence emission with a virtually increased Stokes shift by means of through-space or through-bond energy transfer (EnT) [26–30]. On the one hand, in the latter case electronic communication between the energy-donor antenna and the BODIPY energy acceptor is facilitated in so-called EnT cassettes [12,26–28,31–33]. On the other hand, through-space EnT is classically described by the Förster theory, implying antenna-BODIPY dyads with non-conjugating linkers [29,34–37].

A second strategy which eliminates the mentioned difficulties is the design of two-photon-excitable BODIPY chromophores [3,38–40]. For this purpose, BODIPY dyes are modified with electron-donating aromatic amines and conjugating ethenyl linkers, thereby enabling electronic communication [3,40–42]. These probes were successfully exploited for two-photon-excitation (TPE) fluorescence microscopy for cellular imaging [3,43]. The use of red or near-infrared excitation light sources bears additional

advantages such as deeper penetration into biological tissues, less background fluorescence from biomolecules, and improved photostability of the dyes [23,44,45]. In the light of these two approaches for improved BODIPY dyes in the context of biologically relevant applications we sought to synthesize and characterize a dyad that combines both strategies by means of using a two-photon-excitable antenna to sensitize efficiently BODIPY fluorescence by EnT. Two-photon-induced EnT is less frequently reported and requires a careful selection of the antenna energy donor dye [29,46–48]. Herein we selected a fluorophore class with significant intramolecular charge-transfer (ICT) properties, known to exhibit significant two-photon-absorption cross sections (σ_2): a 2-*N*,*N*-dialkylamino-6-alkanoylnaphthalene derivative. The latter motif is found in archetypal environment-sensitive fluoroprobes such as Prodan (2-dimethylamino-6-propionylnaphthalene) [49], Badan (6-bromoacetyl-2-dimetylaminonaphtalene) [50] or Laurdan (2-dimethylamino-6-lauroylnaphthalene) [51]. These dyes have enjoyed extensive application for the monitoring of the biophysical properties of lipid membranes, including parameters such as polarity, viscosity, and structural order [52–54].

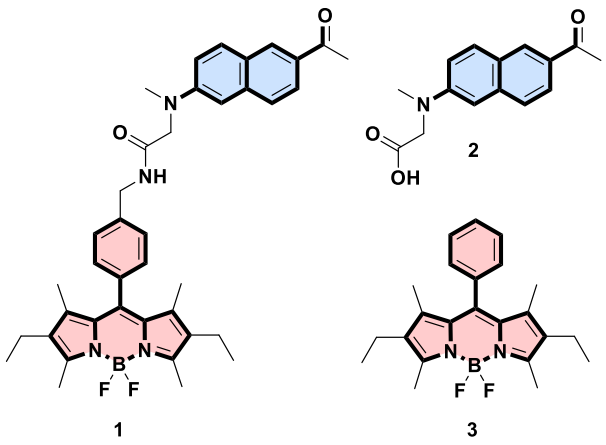

Fig. 1. Structures of the bichromophoric dyad **1** and the individual model chromophores **2** and **3**.

The concrete structures of the herein prepared bichromophoric antenna-BODIPY dyad and the separate chromophore models are shown in Fig. 1. We present their complete photophysical characterization, including the highly efficient EnT-sensitization of the BODIPY fluorescence, the implications of solvatochromic effects on the antenna excited-state properties, and the two-photon-absorption processes. Finally, we demonstrate the internalization of the dyad **1** in N13 microglial cells and proof-of-concept for the validity of the molecular and photophysical design in complex bio-relevant environments.

2. Materials and methods

2.1. General

All reagents and solvents were obtained from commercial sources and were used without further purification unless otherwise stated. Tetrahydrofuran (THF), acetonitrile (MeCN), *N*,*N*-dimethylformamide (DMF), and methanol (MeOH), which were used in the photophysical measurements, were of spectroscopy grade. ^{1}H, ^{13}C, ^{11}B, and ^{19}F NMR spectra were recorded either on a Bruker Advance III 400 MHz or a Bruker Advance III 500 MHz instrument. Structural assignments were made with additional information from gCOSY and gHSQC experiments. Chloroform-*d* and dimethylsulfoxide-d_6 (all 99 atom-% D) were used as solvents, and the spectra were referenced to the residual solvent peak (δ = 7.26 and 2.50 ppm, respectively). High-resolution mass spectrometry (HRMS) was performed using an Elite QTOF, Bruker Daltonics Autoflex ESI-TOF or a Thermo Fisher Orbitrap high-resolution mass spectrometer. Fourier transform infrared spectra (FTIR) were collected on a Bruker Tensor27 spectrometer or an FT/IR 4200 Jasco spectrometer with an attenuated total reflectance (ATR) module. The samples were supported in KBr and the spectra were

recorded in the 500−4000 cm^{-1} wavenumber range. The products were purified by column chromatography or by preparative thin-layer chromatography on silica gel Merck-60 (230-400 mesh, 60 Å) and analytical TLC was performed on aluminum sheets pre-coated with silica gel 60 F_{254} (Merck).

2.2. Synthesis and characterization

4-((2,2,2-Trifluoroacetamido)methyl)benzoic acid **4** [55] (Scheme 1) and the model chromophores Prodan **2** [52] and BODIPY **3** [56] were prepared following reported procedures. The analytical characterization of the final products **2** and **3** revealed their identity and purity (Supplementary Material – Fig. S7–S14, S22–S23, and S27–S28).

*2.2.1. BODIPY **5***

An oven-dried two-neck round-bottom flask, connected to a reflux condenser and held under a nitrogen atmosphere, was charged with the protected amino derivative **4** (150.0 mg, 0.61 mmol). Toluene (10.0 mL) and thionyl chloride (1.0 mL, 13.7 mmol) were added, and the reaction mixture was stirred at 80 ºC for 12 h. The solvent was evaporated under reduced pressure and the residue was dissolved in dry dichloromethane (20 mL). Then kryptopyrrole (0.3 mL, 2.2 mmol) was added and the mixture was refluxed for 4 hours under a nitrogen atmosphere. Subsequently, triethylamine (2.0 mL) and $BF_3{\cdot}OEt_2$ (2.0 mL) were added into the mixture upon which it turned dark red. The reaction mixture was then diluted with dichloromethane (100 mL) and washed with water (2 × 20 mL). The organic layer was dried over anhydrous $MgSO_4$ and the solvent was evaporated under reduced pressure. The crude was purified by silica gel column chromatography (dichloromethane/cyclohexane, 1:1 to pure dichloromethane gradient, R_F = 0.56) affording BODIPY **5** (61 mg, 20% yield) as a red

amorphous solid. ^{1}H NMR (400 MHz, $CDCl_3$, 298 K): δ 7.40 (d, J = 8.0 Hz, 2H), 7.29 (d, J = 8.0 Hz, 2H), 6.90 (br, 1H), 4.63 (d, J = 5.9 Hz, 2H), 2.52 (s, 6H), 2.30 (q, J = 7.5 Hz, 4H), 1.26 (s, 6H), 0.97 (t, J = 7.5 Hz, 6H) ppm (Fig. S15). ^{13}C{^{1}H} NMR (100 MHz, $CDCl_3$, 298 K): δ 158.0, 157.6, 157.2, 156.8, 154.0, 139.3, 138.2, 136.9, 135.8, 133.0, 130.7, 129.0, 128.2, 120.2, 117.3, 114.5, 111.6, 43.4, 17.1, 14.6, 12.5, 11.8 ppm (Fig. S16). HRMS (ESI): Found $[M+H]^+$ 506.2408; molecular formula $C_{26}H_{30}BF_5N_3O$ requires $[M+H]^+$ 506.2397 (Fig. S24). FTIR (ATR) ν_{max}: 3390, 3373, 2965, 2930, 2872, 1727, 1538, 1321, 1190, 1161, 1063, 974, 798, 713, 537 cm^{-1} (Fig. S29).

*2.2.2. BODIPY **6***

An oven-dried 25 mL Schlenk tube was charged with BODIPY **5** (60.0 mg, 0.12 mmol), anhydrous K_2CO_3 (20.0 mg, 0.14 mmol), and 10 mL of a methanol/water mixture (9:1, 10 mL). The solution was stirred at room temperature for 48 hours. The mixture was then concentrated under reduced pressure, re-dissolved in dichloromethane (20 mL), and washed with water (2 × 20 mL). The organic layer was dried over anhydrous $MgSO_4$ and the solvent was evaporated under reduced pressure to afford a red amorphous solid (38 mg, 78% yield) which was used in the next step without further purification. ^{1}H NMR (400 MHz, $CDCl_3$, 298 K): δ 7.44 (d, J = 7.5 Hz, 2H), 7.25 (d, J = 7.5 Hz, 2H), 3.99 (s, 2H), 2.54 (s, 6H), 2.31 (q, J = 7.2 Hz, 4H), 1.30 (s, 6H), 0.99 (t, J = 7.2 Hz, 6H) ppm (Fig. S17). ^{13}C{^{1}H} NMR (100 MHz, $CDCl_3$, 298 K): δ 153.5, 143.8, 140.2, 138.3, 134.1, 132.6, 130.8, 128.3, 127.5, 46.0, 29.6, 17.0, 14.5, 12.4, 11.7 ppm (Fig. S18). HRMS (ESI): Found $[M+H]^+$ 410.2583; molecular formula $C_{24}H_{31}BF_2N_3$ requires $[M+H]^+$ 410.2574 (Fig. S25). FTIR (ATR) ν_{max}: 2964, 2928, 2870, 1671, 1538, 1474, 1319, 1265, 1187, 1061, 975, 758, 710 cm^{-1} (Fig. S30).

*2.2.3. Dyad **1***

An oven-dried 25 mL Schlenk tube was charged with the Prodan derivative **2** (30.0 mg, 0.12 mmol), benzotriazole-1-yl-oxy-tris-pyrrolidino-phosphonium hexafluorophosphate (PyBOP; 62.0 mg, 0.12 mmol), 4-methylmorpholine (NMM; 0.15 mL, 1.37 mmol), and dry dichloromethane (5.0 mL) under nitrogen atmosphere. The mixture was stirred at room temperature for 30 minutes. Subsequently, BODIPY **6** (48 mg, 0.12 mmol) was added in several portions and the reaction mixture was stirred for another 90 minutes at room temperature. The mixture was then diluted with dichloromethane (100 mL). The organic phase was washed with milli-Q water (2 × 20 mL), followed by 0.1 M HCl (2 × 20 mL). The organic layer was dried over anhydrous $MgSO_4$ and the solvent was evaporated under reduced pressure. The crude product was purified by silica gel column chromatography (ethyl acetate/*n*-hexane 4:6), followed by preparative TLC (dichloromethane/methanol 50:1, R_F = 0.69), affording the desired dyad **1** (31 mg, 41%) as red amorphous solid. ^{1}H NMR (500 MHz, $CDCl_3$, 298 K): δ 8.33 (s, 1H), 7.96 (dd, *J* = 8.7, 1H), 7.85 (d, *J* = 9.1 Hz, 1H), 7.68 (d, *J* = 8.7 Hz, 1H), 7.29 (d, *J* = 8.0 Hz, 2H), 7.15 (d, *J* = 8.0 Hz, 2H), 7.11 (dd, *J* = 9.1, 2.6 Hz, 1H), 7.00 (s, 1H), 6.83 (t, *J* = 6.1 Hz, 1H), 4.60 (d, *J* = 6.1 Hz, 2H), 4.14 (s, 2H), 3.21 (s, 3H), 2.66 (s, 3H), 2.51 (s, 6H), 2.25 (q, *J* = 7.5 Hz, 4H), 1.11 (s, 6H), 0.95 (t, *J* = 7.5 Hz, 6H) ppm (Fig. S1). ^{13}C{^{1}H} NMR (126 MHz, $CDCl_3$, 298 K): δ 197.7, 169.9, 154.0, 148.8, 139.7, 139.0, 138.3, 137.3, 135.2, 132.9, 132.2, 131.4, 130.8, 130.1, 128.8, 128.0, 126.7, 126.4, 125.3, 116.2, 107.1, 58.5, 42.9, 40.2, 26.6, 17.2, 14.7, 12.6, 11.8 ppm (Fig. S3). ^{11}B NMR (160 MHz, $CDCl_3$, 298 K): δ 0.77 (t, *J* = 33.6 Hz) ppm (Fig. S5). ^{19}F NMR (470 MHz, $CDCl_3$, 298 K): δ –145.81 (q, *J* = 32.4 Hz) ppm (Fig. S6). HRMS (ESI): Found $[M+Na]^+$ 671.3395; molecular formula $C_{39}H_{43}BF_2N_4O_2$ requires $[M+Na]^+$ 671.3346 (Fig. S20). FTIR (KBr)

ν_{max}: 3413, 2959, 2924, 2855, 1665, 1621, 1461, 1378, 1261, 1095, 1021, 801 cm^{-1} (Fig. S26).

2.3. Photophysical measurements

All photophysical measurements were performed at room temperature (293 K) with 10 µM solutions, contained in quartz cuvettes (1 cm optical pathlength). UV/Vis absorption spectra were measured with a UVPC-1603 instrument from Shimadzu. Steady-state fluorescence measurements were done on a Varian Eclipse fluorimeter. The fluorescence spectra were corrected for the spectral responsivity of the photomultiplier-based detection system by applying an emission correction curve. Fluorescence quantum yields were determined for diluted sample solutions (absorbance of ≤ 0.1 at the excitation wavelength) and by using rhodamine 6G in ethanol ($\Phi_f = 0.95$) [57] or quinine sulfate in 0.05 M H_2SO_4 as reference ($\Phi_f = 0.55$) [58]. The quantum yields were calculated by taking the refractive indices of the employed solvents into account [59]. The two-photon absorption cross-sections (σ) were determined according to a standard two-photon excited-fluorescence method [60]. The experiments were done within a laser-power regime where the fluorescence is proportional to the square of the laser excitation power. As reference a rhodamine B solution (10 µM in MeOH) was used [60], reasonably assuming that the fluorescence quantum yield is the same regardless of one- or two- photon excitation. The two-photon-excited fluorescence of dyad **1** was analysed using an inverted Leica SP5 MP confocal microscope equipped with a MaiTai Ti:Sapphire HP laser (Spectra-Physics, Inc.), tuneable between 690 and 1040 nm. Emission spectra were measured using a dynamic 10 nm wide emission detection window moving in 28 steps between 425 and 705 nm.

Time-correlated single-photon-counting measurements were performed on a FS920 fluorescence spectrometer (Edinburgh Instruments). As excitation sources, picosecond pulsed diode lasers (Edinburgh Instruments) were used (EPL-445: λ_{exc} = 442.2 nm, pulse width 78.3 ps; EPL-485: λ_{exc} = 482.0 nm, pulse width 100.6 ps). The nanosecond fluorescence decays were deconvoluted, using the instrument response function that was recorded with a light-scattering Ludox solution.

2.4. DFT calculations

All calculations were done with the Gaussian 09 package [61]. The solvent effect was considered by including the polarizable continuum model (PCM) [62] and MeCN as the solvent. The starting geometries for the calculations were first optimized using AM1 followed by density functional theory (DFT). The ground-state (S_0) geometrical parameters have been determined with the density functional level of theory, without symmetry constraints and employing the Coulomb-attenuated CAM-B3LYP functional and the 6-31+G(d) basis set. Using the optimized ground-state geometries as starting coordinates, time-dependent density-functional-theory (TD-DFT) geometry optimizations of the (S_1) states were performed, using the first ten excited states and the linear-response (LR-PCM) approach. On these optimized structures, the state-specific model (SS-PCM) has been evaluated considering an equilibrated state between the solvent and the excited-state electron density.

The orientation factor (κ^2) is defined by $\kappa^2 = (cos\theta_T - 3cos\theta_D cos\theta_A)^2$, where θ_T is the angle between the emission transition dipole of the donor and the absorption transition dipole of the acceptor, θ_D and θ_A are the angles between these dipoles and the vector joining the donor and acceptor [59]. The calculation of the orientation factor requires the transition dipole moment vectors of the donor and acceptor moieties, which

were obtained by carrying out TD-DFT (CAM-B3LYP/6-31+G(d) level of theory, first ten excited states). Once the transition electric dipole moment vector coordinates were obtained, these coordinates were appended on the optimized geometry of the molecule. The centers of the individual donor and acceptor moieties were joined and all the angles that are necessary to calculate the orientation factor were obtained.

2.5. Bioimaging experiments

N13 microglial cells were grown to 50–70 % confluence on 8-well slides at 37 ºC with 5% CO_2 in Gibco RPMI 1640 medium supplemented with *L*-glutamine and fetal bovine serum. The N13 microglial cells were incubated for 1 hour with 1 mL of fresh, preheated RPMI 1640 culture medium containing varying concentrations (100 µM, 10 µM, 1 µM) of dyad **1** prepared from a stock solution ([**1**] = 2.1 mM) in DMSO. The intracellular fluorescence of dyad **1** was analysed using an inverted Leica SP5 MP and a HCX IRAPO L 25.0 × 0.95 WATER objective. Optimal conditions were maintained throughout the imaging process with an integrated microscope enclosure keeping cells at 37 ºC and 5% CO_2. Dyad **1** was visualized using two-photon excitation at 750 nm and fluorescence detection between 425–705 nm using a HyD non-descanned detector. Brightfield images were captured independently using a 405-nm laser as light source.

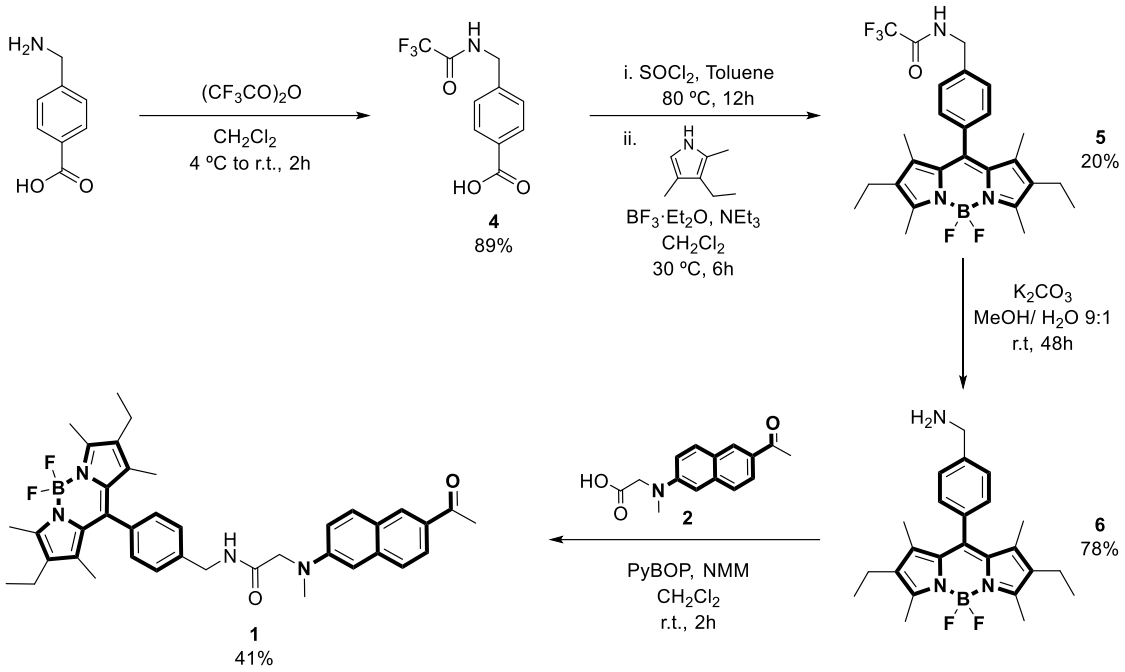

Scheme 1. Synthesis of dyad **1**.

3. Results and discussion

*3.1. Synthesis of dyad **1***

The bichromophoric dyad **1** was synthesized in a three-step sequence (Scheme 1) starting by preparation of the trifluoroacetyl-protected amino-BODIPY derivative **5** by means of an activation of the previously described protected *p*-aminobenzoic acid derivative **4** [55] in form of its acyl chloride (reaction with $SOCl_2$), reaction with kryptopyrrole, and finally treatment with $BF_3{\cdot}OEt_2$ and NEt_3 as base. In the next step, the deprotection of the amino group was carried out under basic conditions (K_2CO_3) to obtain the BODIPY derivative **6**. In the final step **6** was then reacted with the known Prodan-derived antenna chromophore **2** [52] by means of a standard amidation protocol with the coupling reagents 4-methylmorpholine and PyBOP. This yielded the bichromophoric dyad **1**, containing a hydrolytically stable amide linker. Column chromatography on silica gel, followed by a second repurification by preparative TLC, yielded an analytical pure sample (see the Supplementary Material for details on the

detailed 1D and 2D NMR-spectroscopic characterization, signal assignments, and high-resolution mass spectrometry data).

3.2. Optical spectroscopy and excited-state processes on one-photon excitation (OPE)

In order to account for the known solvatochromic effects of Prodan-like chromophores, such as the herein employed antenna, we used solvents of varying polarity in the present study: acetonitrile (MeCN), tetrahydrofuran (THF), *N*,*N*-dimethylformamide (DMF), and methanol (MeOH). All photophysical data are summarized in Table 1. The normalized UV/Vis-absorption and emission spectra of the dyad **1** and the model chromophores (**2** and **3**) in MeCN are shown in Fig. 2 and Fig. 3, respectively (see the Supplementary Material for the other solvents – Fig. S31–S32).

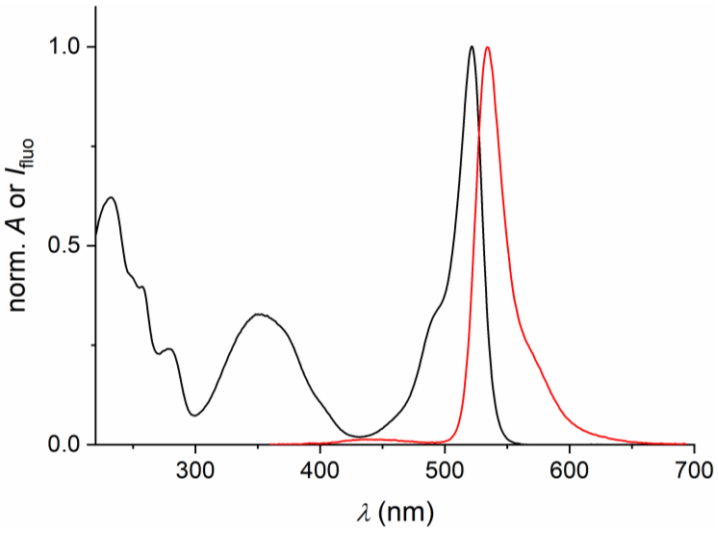

Fig. 2. UV/Vis absorption (black line) and fluorescence (red line; excitation at 350 nm) spectra of dyad **1** (10 µM) in MeCN.

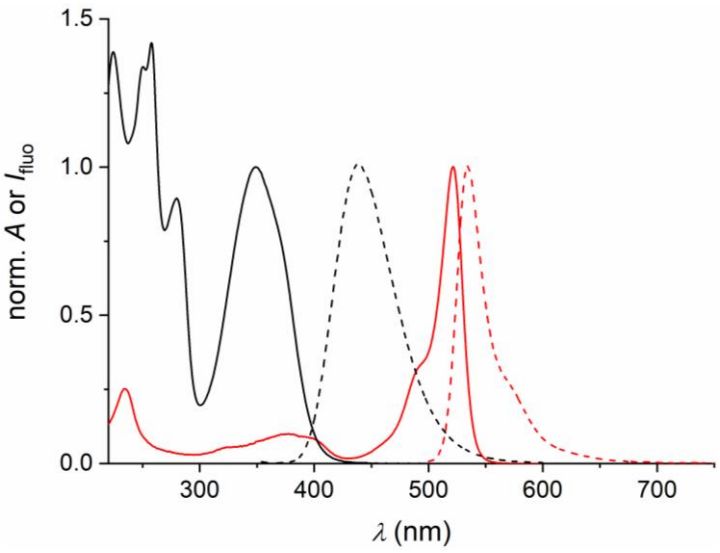

Fig. 3. UV/Vis absorption (solid line) and fluorescence (dashed line) spectra of model chromophores **2** (black) and **3** (red) (10 μM each) in MeCN. The fluorescence spectra were obtained by excitation at 350 nm (**2**) or 495 nm (**3**).

Expectedly, only the Prodan-derived dye **2** and the corresponding part of dyad **1** showed significant solvatochromic effects of the absorption maxima, while the BODIPY chromophore exhibited the widely known polarity-independent spectral features. For dye **2** this is experimentally underpinned by a bathochromic red shift of about 30 nm upon changing from the less polar THF to the highly polar MeOH. Similar trends were observed for dyad **1**, with significant shifts of the longest wavelength absorption of the ICT chromophore ($\Delta\lambda$ = +15 nm for MeOH *versus* THF) and practically solvent-independent absorption spectral features of the BODIPY moiety.

Table 1. Photophysical properties of **1**–**3** in various solvents.

	Solvent	λ_{abs} (nm) [ε ($M^{-1}cm^{-1}$)]	λ_{fluo} (nm)	Φ_{fluo}	τ_{fluo} (ns)
1	MeCN	350 [21700]	534[a]	0.21[b]	2.43[b]
		522 [64000]		0.33[c]	2.45[c,d]
	THF	348 [19800]	537[a]	0.53[b]	5.00[b]
		524 [74200]		0.77[c]	5.14[c]
	DMF	356 [22200]	538[a]	0.20[b]	2.53[b]
		524 [66100]		0.34[c]	2.62[c,d]
	MeOH	363 [19900]	536	0.36[b]	3.67[b]
		523 [67300]		0.52[c]	3.66[c]
2	MeCN	349 [19100]	440	0.73	3.05
	THF	349 [19000]	422	0.55	2.58[d]
	DMF	362 [19100]	450	0.62	3.22
	MeOH	378 [19700]	502	0.26	2.52[d]
3	MeCN	521 [69600]	535	0.80	5.56
	THF	524 [69900]	538	0.82	3.92
	DMF	524 [77800]	537	0.77	5.14
	MeOH	522 [74000]	534	0.84	5.78

[a] A very minor band corresponding to the antenna fluorescence was noted. THF: λ_{fluo} = 423 nm (I_{537}/I_{423} = 250); MeCN: λ_{fluo} = 439 nm (I_{534}/I_{439} = 71); DMF: λ_{fluo} = 452 nm (I_{538}/I_{452} = 25). [b] Values correspond to the excitation of the antenna chromophore at 350 nm. [c] Values correspond to the direct excitation of the BODIPY chromophore at 495 nm. [d] Biexponential decay; the average lifetime is given.

Furthermore, the UV/Vis absorption spectrum of the dyad resembles the sum of the two model chromophores and the high molar absorption coefficients of each moiety are also observed for the dyad (see Table 1). This corroborates the independence of the ground-state chromophores in **1**, which is an expected finding for an electronically isolating linker as the one employed herein.

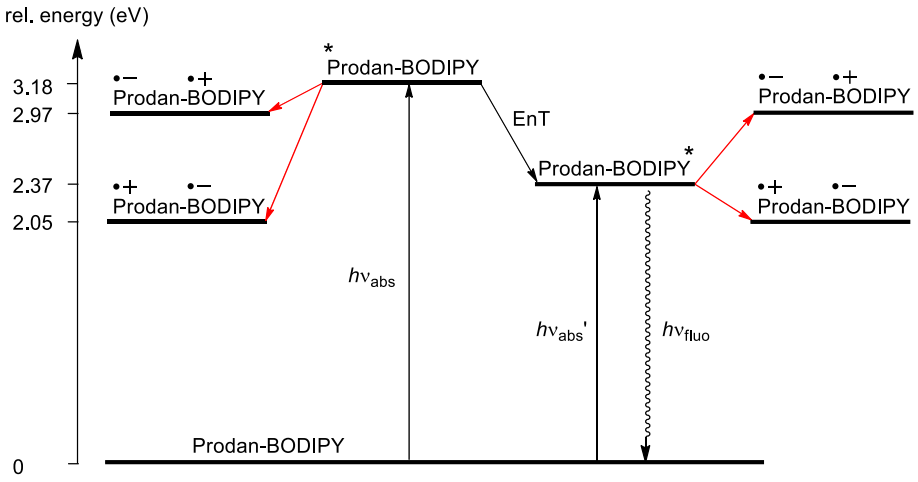

Fig. 4. Quantitative energy diagram depicting the hypothetic photoinduced electron transfer pathways (red arrows) in dyad **1**. Redox potentials (vs. SCE, in MeCN): E_{ox} (Prodan) = +0.74 V [63], E_{ox} (BODIPY) = +0.94 V [64], E_{red} (Prodan) = –2.09 V [65], E_{red} (BODIPY) = –1.37 V [64]. Excitation energies: E^* (Prodan) = 3.18 eV (calculated as average of energy of absorption and emission maximum; see ref. [66]), E^* (BODIPY) = 2.37 eV [64].

Regarding the fluorescence properties, the models **2** and **3** show again their characteristic behavior in solvents of different polarity: a bathochromic shift in polar solvents for the ICT chromophore **2** (up to 80 nm on going from THF to MeOH) and indifferent emission features of the BODIPY **3**. Strikingly, in the dyad **1** the fluorescence of the Prodan chromophore is hardly visible on its selective excitation (at 350 nm *ca*. 80% of the absorbed photons correspond to the Prodan-derived moiety), being in agreement with efficient quenching by excited state communication with the BODIPY chromophore (see Fig. 2). Instead practically only the BODIPY emission is observed, exhibiting the same spectral features as obtained for the direct excitation of the boron-containing fluorophore at 495 nm. This hints on an efficient quenching process involving excited-state EnT, where the ICT chromophore plays the role of the

energy donor and the BODIPY is the acceptor (see below). In comparison to model **3** the fluorescence quantum yields on direct excitation of the BODIPY in dyad **1** remain high in non-polar THF (0.77 for **1** *versus* 0.82 for **3**), but are considerably lower in polar solvents (*ca*. 0.3 for **1** *versus ca*. 0.8 for **3** in MeCN or DMF). Similar quenching effects are expressed by the decreased BODIPY fluorescence lifetimes of **1** in polar solvents. This fluorescence quenching is even more accentuated when exciting the Prodan-derived chromophore moiety instead, with BODIPY fluorescence quantum yields that are significantly smaller than measured for the direct BODIPY excitation in the dyad (see Table 1). The pronounced solvent dependence of these effects provides a hint that photoinduced electron transfer (PeT) pathways may be at their origin. This possibility was more carefully examined by taking into account the thermodynamic feasibility of the different PeT pathways (see Fig. 4). The driving force ΔG_{PeT} for the different PeT pathways was estimated by means of the Rehm-Weller equation [Eq. 1; E_{ox} – oxidation potential of electron donor, E_{red} – reduction potential of the electron acceptor, E^* – singlet excitation energy, C – Coulomb term (–0.06 eV in MeCN)] [67].

$$\Delta G_{PeT} = E_{ox} - E_{red} - E^* + C \quad \text{(Eq. 1)}$$

The oxidative and reductive electron-transfer fluorescence quenching of the ICT chromophore are exergonic processes (ΔG_{PeT} = –1.13 eV and –0.21 eV, respectively) and thereby energetically allowed. Along the same lines of thought, the reduced BODIPY fluorescence quantum yield obtained on direct excitation can be reasoned with an exergonic reductive PeT (ΔG_{PeT} = –0.32 eV), while the oxidative pathway would be thermodynamically disfavored (ΔG_{PeT} = +0.60 eV). Based on this analysis, it reasonable to assume that in polar solvents PeT competes with the EnT process and leads to the

observed quenching of BODIPY fluorescence (generated by direct excitation or by the EnT-sensitized pathway).

Table 2. Parameters of Förster resonance energy transfer in dyad **1** in various solvents.

	MeCN	THF	DMF	MeOH
$J \times 10^{-11}$ (cm^6mol^{-1})[a]	4.0	1.8	5.9	16
R_0 (Å)[b]	35.3	28.6	35.2	37.7
$k_{EnT} \times 10^{11}$ (s^{-1})[c]	7.6	2.5	7.1	14
Φ_{EnT}[d]	1	1	1	1

[a] Spectral overlap integral between donor emission and acceptor absorption spectra (see Eq. 2). [b] Critical FRET radius (see Eq. 3), with $\kappa^2 = 0.2461$. [c] Energy-transfer rate constant (see Eq. 4). [d] Energy-transfer quantum yield (see Eq. 5).

Albeit the above discussed PeT pathways interfere in the excited-state behavior of **1** (especially in polar solvents), it is clear from the abovementioned observations that excitation of the Prodan-derived moiety leads to the observation of BODIPY fluorescence emission. This can be only reasonably explained with EnT communication between both chromophores. With the objective to shine more light on this process, a more detailed analysis according to the Förster theory of resonance energy transfer (FRET) was undertaken [68]. The key data, such as the spectral overlap integral J, the critical transfer radius R_0, the quantum yield Φ_{EnT}, and the rate constant k_{EnT} of energy transfer are summarized in Table 2; see equations 2–5.

$$J = \int_0^\infty [F_D(\nu)\varepsilon_A(\nu)d\nu]/\nu^4 \qquad \text{(Eq. 2)}$$

$$R_0^6 = 8.8 \times 10^{-28}\ \Phi_D\ \kappa^2\ n^{-4}\ J \qquad \text{(Eq. 3)}$$

$$\Phi_{EnT} = 1/[1 + (R/R_0)^6] \qquad \text{(Eq. 4)}$$

$$k_{\mathrm{EnT}} = (1/\tau_{\mathrm{D}}) \times (R_0/R)^6 \qquad \text{(Eq. 5)}$$

The actual center-to-center distance of the donor and acceptor units, obtained from molecular dynamics simulations (see details in the Supplementary Material), accounting for the conformational flexibility of the linker, is significantly smaller than the critical transfer radius, e.g., 9.8 Å *versus* 35.3 Å in MeCN. This leads to the prediction of practically quantitative inherent EnT (Φ_{EnT} *ca*. 1), independent on the polarity of the solvent. In practice, PeT (see above) competes with this process, thereby lowering the quantum yields of sensitized BODIPY fluorescence in polar solvents. However, in all solvents the EnT is evidently operative and in essence the relatively small Stokes shift of the BODIPY chromophore itself (*ca*. 10 nm) is considerably enlarged to *ca*. 170–180 nm in the dyad, referring to an apparent Stokes shift.

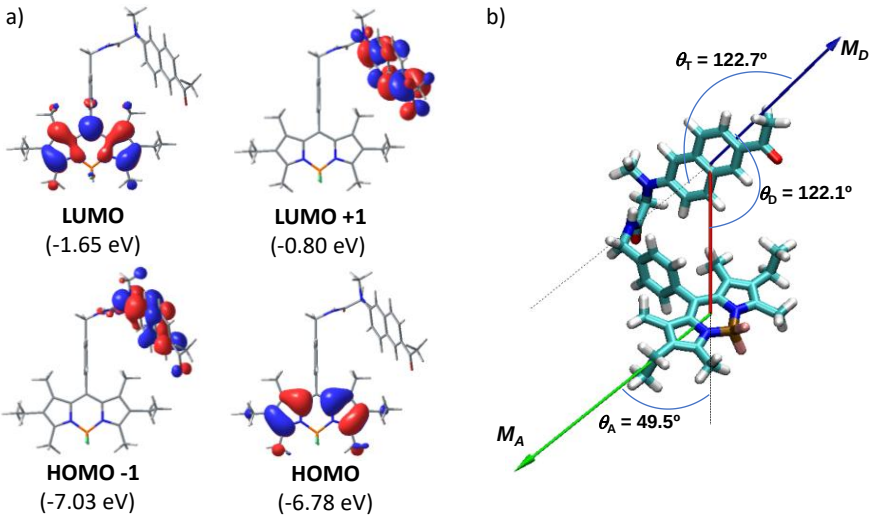

Fig. 5. (a) Contour plots of relevant frontier orbitals of dye **1**, and (b) Optimized ground-state geometry showing data for calculation of the orientation factor κ^2 corresponding to dyad **1**.

Table 3. Main absorption and emission transitions of dyad **1** and the corresponding model compounds **2** and **3**.

Dyad 1	**2**	**3**
Absorption		
$S_1 \leftarrow S_0$ (f = 0.680)[a] LUMO ← HOMO (98%) E = 2.92 (2.38)[b] eV		$S_1 \leftarrow S_0$ (f = 0.691)[a] LUMO ← HOMO (98%) E = 2.92 (2.38)[b] eV
$S_3 \leftarrow S_0$ (f = 0.472)[a] LUMO+1 ← HOMO–1 (90%) E = 3.70 (3.54)[b] eV	$S_1 \leftarrow S_0$ (f = 0.487)[a] LUMO ← HOMO (90%) E = 3.66 (3.55)[b] eV	
Emission		
$S_1 \rightarrow S_0$ (f = 0.837)[a] LUMO → HOMO (98%) E = 2.80 (2.32)[b] eV		$S_1 \rightarrow S_0$ (f = 0.840)[a] LUMO → HOMO (98%) E = 2.80 (2.32)[b] eV
$S_3 \rightarrow S_0$ (f = 0.728)[a] LUMO+1 → HOMO–1 (93%) E = 2.98 (2.82)[b] eV	$S_1 \rightarrow S_0$ (f = 0.808)[a] LUMO → HOMO (96%) E = 2.99 (2.82)[b] eV	

[a] Oscillator strength f. [b] In parenthesis the experimental transition energy, based on the absorption and emission maxima, is given.

3.3. Theoretical calculations

The electronic independence of the two chromophores in dyad **1** was confirmed by time-dependent density functional theory (TD-DFT) calculations at the CAM-B3LYP/6-31+G(d) level of theory. The solvent (MeCN) was taken into account by means of the polarizable continuum model (PCM). The calculations confirmed orthogonal chromophore-specific transitions with no sign of mixing: $S_3 \leftarrow S_0$, dominated by LUMO+1←HOMO−1 (90% weighted contribution) for the Prodan-derived moiety and $S_1 \leftarrow S_0$, dominated by LUMO←HOMO (98% weighted contribution) for the BODIPY moiety (see Fig. 5). The corresponding frontier molecular orbitals (FMO) are localized on the respective chromophoric unit, which clearly underpins the electronic insulation by the non-conjugative linker. The calculated excitation and emission energies of **1** express the experimentally verified trends correctly (see Table 3). Further,

a comparison with the calculated data for the models **2** and **3** underpins the electronic orthogonality of the two chromophores in dyad **1** (Supplementary Material – Fig. S33–S34).

3.4. Two-photon excitation (TPE)

The electronic constellation of the Prodan-derived antenna chromophore, being a push-pull architecture, opens the possibility for exploring two-photon absorption (TPA) processes and their implication in the EnT-sensitized generation of BODIPY fluorescence. As exemplified for model compound **3**, the plain BODIPY chromophore is a rather inefficient two-photon absorber (<10 GM at wavelengths between 740 and 1040 nm). However, by the target-oriented design of electronic properties an improvement of the TPA properties of BODIPY dyes can be achieved [3,69,70]. The herein followed strategy is different. It relies on the two-photon-induced population of the first excited singlet state of the antenna chromophore that engages subsequently in the same EnT process as observed under one-photo-excitation (OPE) conditions (see above). The TPA action spectrum of dyad **1** in DMF was obtained by the comparative method using rhodamine B as reference (see Materials and methods). The data are shown in Fig. 6. Two spectrally well differentiated maxima at 700 nm and 970 nm are observed. In agreement with the spectra that are known for the two separate moieties of the dyad (see Fig. 6) these bands are assigned to the Prodan-derived antenna chromophore and the BODIPY moiety, respectively. Having in mind that the BODIPY fluorescence quantum yield varies in dependence on the fact whether it was generated by a sensitization mechanism or direct excitation (see above), the absolute two-photon cross section σ_2 of the antenna part is calculated as 293 GM at 700 nm and the one of the BODIPY moiety as 32 GM at 970 nm (1 GM = 10^{-50} cm^4 s $photon^{-1}$). The BODIPY

emission spectra that are obtained on excitation in either TPA band (at 700 nm or 1000 nm) are identical (see Fig. S37 in the Supplementary Material), showing the typical narrow-shaped profile and a maximum at *ca*. 540 nm. Akin to the observations made for OPE (see above), for the excitation of the Prodan-derived moiety at 700 nm a very minor emission with a maximum around 455 nm was seen. These joint observations underpin our notion of the operation of the same EnT process that was characterized in detail for the OPE conditions (see above). In fact, the attachment of the Prodan-derived antenna does not only increase the apparent Stokes shift (see above) of the BODIPY dye, but also improves indirectly its TPA properties by means of the antenna effect.

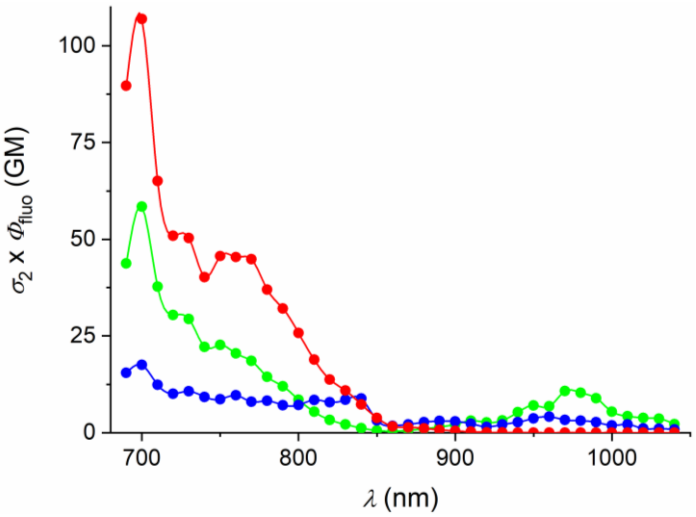

Fig. 6. Two-photon absorption spectra for bichromophoric dyad **1** (green), and models **2** (red) and **3** (blue) in DMF (10 µM each).

*3.5. Cellular imaging with dyad **1***

With view on potential bioimaging applications dyad **1** was investigated regarding the operation of the two-photon-induced EnT in the environment of the N13 microglial cells. The incubation of dyad **1** with N13 microglial cells, following a standard protocol (see Materials and methods), and subsequent fluorescence imaging on excitation at 750

nm (absorbed predominantly by the Prodan-derived moiety) yielded well resolved images that evidenced the successful cellular uptake of the probe and its accumulation in the cytoplasm (see Fig. 7 and the Supplementary Material for bright-field images – Fig. S38). The brightness of the dyad is sufficiently high to lower the concentration of the dye in the incubation broth down to 1 µM.

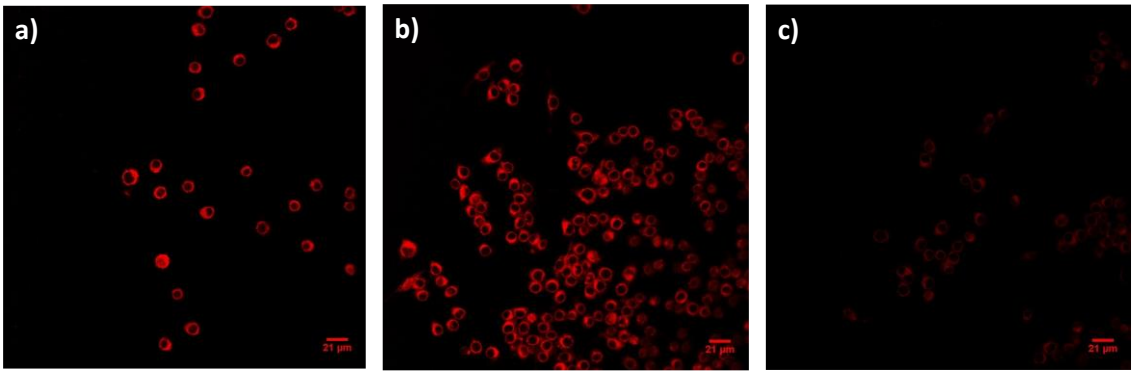

Fig. 7. Two-photon confocal microscopy images of N13 microglial cells incubated with dyad **1** in different concentrations; excitation at 750 nm. Concentrations of **1**: 100 µM (a), 10 µM (b), 1 µM (c).

The *in cellulo* detected fluorescence spectrum revealed the typical narrow emission band of the BODIPY with a maximum at about 540 nm (see Fig. 8). Furthermore, the two-photon excitation spectrum showed a strong band with a maximum at *ca*. 720 nm and a smaller shoulder at *ca*. 790 nm, assigned to the Prodan-derived chromophore (see Fig. 8). The BODIPY chromophore was represented by a weak band at *ca*. 990 nm. These features coincide with the observations in solution. Hence, it can be safely concluded that the photophysical key features of the bichromophoric dyad **1**, namely TPA and the EnT communication, persist under the experimental conditions of fluorescence imaging in the model cell line.

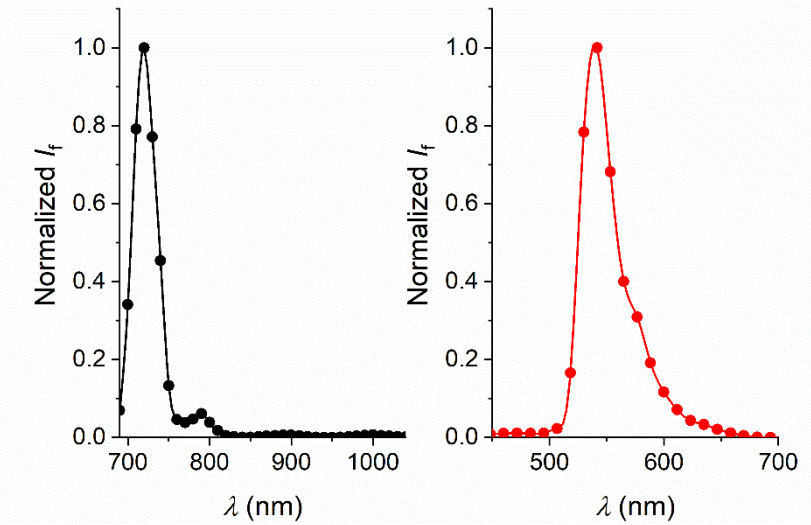

Fig. 8. Left: Two-photon excitation spectrum of **1**, incubated with N13 microglial cells (monitoring of emission between 542 and 572 nm). Right: Corresponding emission spectrum, excitation at 750 nm.

Conclusions

The combination of a two-photon-absorbing antenna Prodan dye with a BODIPY fluorophore permitted the demonstration of the EnT-sensitized fluorescence emission of the latter on excitation of the antenna with near-infrared photons. The EnT is predicted to be highly efficient. However, in polar solvents the competition with PeT processes adds some complexity to the excited state characteristics. The EnT-sensitization is still operative *in cellulo*, which permits the use of the dyad in bioimaging.

CRediT authorship contribution statement

Antonio Dominguez-Alfaro: Investigation. **Vânia Pais**: Investigation, Validation. **David B. Guzmán-Ríos**: Investigation, Writing - Review & Editing. **Daniel Collado**: Investigation. **Francisco Nájera**: Investigation, Writing - Review & Editing. **Ezequiel**

Pérez-Inestrosa: Supervision, Writing - Review & Editing. **Uwe Pischel**: Conceptualization, Supervision, Writing - Original Draft.

Declaration of competing interest

The authors declare that they have no competing financial interests or personal relationships that could have influenced the work reported in this paper.

Acknowledgements

We are grateful to the Spanish *Ministerio de Ciencia e Innovación* (grant PID2020-119992GB-I00 for U.P., PID2019-104293GB-I00 for F.N. and E.P.-I.), the European Research and Development Fund (ERDF), the *Junta de Andalucía*/University of Málaga (grant UMA18-FEDERJA-007 for F.N. and E.P.-I.), and the *Junta de Andalucía*/University of Huelva (grant UHU-202070 for U.P.) for providing financial support. We also acknowledge the Supercomputing and Bioinformatics Centre (SCBI) of the University of Málaga for providing the computer resources used for the theoretical calculations.

Appendix A. Supplementary data

Supplementary data to this article can be found online at https://doi. org/...

References

[1] Han J, Loudet A, Barhoumi R, Burghardt RC, Burgess K. A Ratiometric pH Reporter For Imaging Protein-dye Conjugates In Living Cells. J Am Chem Soc 2009;131:1642–3. https://doi.org/10.1021/ja8073374.

[2] Wu L, Loudet A, Barhoumi R, Burghardt RC, Burgess K. Fluorescent Cassettes for Monitoring Three-Component Interactions in Vitro and in Living Cells. J Am Chem Soc 2009;131:9156–7. https://doi.org/10.1021/ja9029413.

[3] Didier P, Ulrich G, Mély Y, Ziessel R. Improved push-pull-push E-Bodipy fluorophores for two-photon cell-imaging. Org Biomol Chem 2009;7:3639–42. https://doi.org/10.1039/B911587K.

[4] Kolemen S, Işık M, Kim GM, Kim D, Geng H, Buyuktemiz M, Karatas T, Zhang XF, Dede Y, Yoon J, Akkaya EU. Intracellular Modulation of Excited-State Dynamics in a Chromophore Dyad: Differential Enhancement of Photocytotoxicity Targeting Cancer Cells. Angew Chem Int Ed 2015;54:5340–4. https://doi.org/https://doi.org/10.1002/anie.201411962.

[5] Kowada T, Maeda H, Kikuchi K. BODIPY-based probes for the fluorescence imaging of biomolecules in living cells. Chem Soc Rev 2015;44:4953–72. https://doi.org/10.1039/C5CS00030K.

[6] Gong D, Tian Y, Yang C, Iqbal A, Wang Z, Liu W, Qin W, Zhu X, Guo H. A fluorescence enhancement probe based on BODIPY for the discrimination of cysteine from homocysteine and glutathione. Biosens Bioelectron 2016;85:178–83. https://doi.org/10.1016/J.BIOS.2016.05.013.

[7] Patalag LJ, Ahadi S, Lashchuk O, Jones PG, Ebbinghaus S, Werz DB. GlycoBODIPYs: Sugars Serving as a Natural Stock for Water-soluble Fluorescent Probes of Complex Chiral Morphology. Angew Chem Int Ed 2021;60:8766–71. https://doi.org/https://doi.org/10.1002/anie.202016764.

[8] Wang D, Miyamoto R, Shiraishi Y, Hirai T. BODIPY-Conjugated Thermoresponsive Copolymer as a Fluorescent Thermometer Based on Polymer Microviscosity. Langmuir 2009;25:13176–82. https://doi.org/10.1021/la901860x.

[9] Zhang J, Yang M, Li C, Dorh N, Xie F, Luo FT, Tiwari A, Liu H. Near-infrared fluorescent probes based on piperazine-functionalized BODIPY dyes for sensitive detection of lysosomal pH. J Mater Chem B 2015;3:2173–84. https://doi.org/10.1039/C4TB01878H.

[10] Gong D, Cao T, Han SC, Zhu X, Iqbal A, Liu W, Qin W, Guo H. Fluorescence enhancement thermoresponsive polymer luminescent sensors based on BODIPY for intracellular temperature. Sens Actuators B Chem 2017;252:577–83. https://doi.org/10.1016/J.SNB.2017.06.041.

[11] Bozdemir OA, Guliyev R, Buyukcakir O, Selcuk S, Kolemen S, Gulseren G, Nalbantoglu T, Boyaci H, Akkaya EU. Selective Manipulation of ICT and PET Processes in Styryl-Bodipy Derivatives: Applications in Molecular Logic and Fluorescence Sensing of Metal Ions. J Am Chem Soc 2010;132:8029–36. https://doi.org/10.1021/ja1008163.

[12] Fan J, Hu M, Zhan P, Peng X. Energy transfer cassettes based on organic fluorophores: construction and applications in ratiometric sensing. Chem Soc Rev 2013;42:29–43. https://doi.org/10.1039/C2CS35273G.

[13] Zhu H, Fan J, Wang B, Peng X. Fluorescent, MRI, and colorimetric chemical sensors for the first-row d-block metal ions. Chem Soc Rev 2015;44:4337–66. https://doi.org/10.1039/C4CS00285G.

[14] Alnajjar MA, Bartelmeß J, Hein R, Ashokkumar P, Nilam M, Nau WM, Rurack K, Hennig A. Rational design of boron-dipyrromethene (BODIPY) reporter dyes for cucurbit[7]uril. Beilstein J Org Chem 2018;14:1961–71. https://doi.org/10.3762/bjoc.14.171.

[15] Gorman A, Killoran J, O'Shea C, Kenna T, Gallagher WM, O'Shea DF. In Vitro Demonstration of the Heavy-Atom Effect for Photodynamic Therapy. J Am Chem Soc 2004;126:10619–31. https://doi.org/10.1021/ja047649e.

[16] McDonnell SO, Hall MJ, Allen LT, Byrne A, Gallagher WM, O'Shea DF. Supramolecular Photonic Therapeutic Agents. J Am Chem Soc 2005;127:16360–1. https://doi.org/10.1021/ja0553497.

[17] Kamkaew A, Lim SH, Lee HB, Kiew LV, Chung LY, Burgess K. BODIPY dyes in photodynamic therapy. Chem Soc Rev 2013;42:77–88. https://doi.org/10.1039/C2CS35216H.

[18] Filatov MA, Karuthedath S, Polestshuk PM, Savoie H, Flanagan KJ, Sy C, Sitte E, Telitchko M, Laquai F, Boyle RW, Senge MO. Generation of Triplet Excited States via Photoinduced Electron Transfer in meso-anthra-BODIPY: Fluorogenic Response toward Singlet Oxygen in Solution and in Vitro. J Am Chem Soc 2017;139:6282–5. https://doi.org/10.1021/jacs.7b00551.

[19] Radunz S, Wedepohl S, Röhr M, Calderón M, Tschiche HR, Resch-Genger U. pH-Activatable Singlet Oxygen-Generating Boron-dipyrromethenes (BODIPYs) for Photodynamic Therapy and Bioimaging. J Med Chem 2020;63:1699–708. https://doi.org/10.1021/acs.jmedchem.9b01873.

[20] Loudet A, Burgess K. BODIPY dyes and their derivatives: Syntheses and spectroscopic properties. Chem Rev 2007;107:4891–932. https://doi.org/10.1021/cr078381n.

[21] Ulrich G, Ziessel R, Harriman A. The Chemistry of Fluorescent Bodipy Dyes: Versatility Unsurpassed. Angew Chem Int Ed 2008;47:1184–201. https://doi.org/https://doi.org/10.1002/anie.200702070.

[22] Boens N, Leen V, Dehaen W. Fluorescent indicators based on BODIPY. Chem Soc Rev 2012;41:1130–72. https://doi.org/10.1039/C1CS15132K.

[23] Lu H, Mack J, Yang Y, Shen Z. Structural modification strategies for the rational design of red/NIR region BODIPYs. Chem Soc Rev 2014;43:4778–823. https://doi.org/10.1039/C4CS00030G.

[24] Li FZ, Yin JF, Kuang GC. BODIPY-based supramolecules: Construction, properties and functions. Coord Chem Rev 2021;448:214157. https://doi.org/10.1016/J.CCR.2021.214157.

[25] Hu D, Zhang T, Li S, Yu T, Zhang X, Hu R, Feng J, Wang S, Liang T, Chen J, Sobenina LN, Trofimov BA, Li Y, Ma J, Yang G. Ultrasensitive reversible chromophore reaction of BODIPY functions as high ratio double turn on probe. Nat Commun 2018;9:362. https://doi.org/10.1038/s41467-017-02270-0.

[26] Ziessel R, Goze C, Ulrich G, Césario M, Retailleau P, Harriman A, Rostron JP. Intramolecular Energy Transfer in Pyrene–Bodipy Molecular Dyads and Triads. Chem Eur J 2005;11:7366–78. https://doi.org/https://doi.org/10.1002/chem.200500373.

[27] Harriman A, Izzet G, Ziessel R. Rapid Energy Transfer in Cascade-Type Bodipy Dyes. J Am Chem Soc 2006;128:10868–75. https://doi.org/10.1021/ja0631448.

[28] Ziessel R, Ulrich G, Olivier JH, Bura T, Sutter A. Carborane-Bodipy scaffolds for through space energy transfer. Chem Commun 2010;46:7978–80. https://doi.org/10.1039/C0CC02656E.

[29] Collado D, Remón P, Vida Y, Najera F, Sen P, Pischel U, Perez-Inestrosa E. Energy Transfer in Aminonaphthalimide-Boron-Dipyrromethene (BODIPY) Dyads upon One- and Two-Photon Excitation: Applications for Cellular Imaging. Chem Asian J 2014;9:797–804. https://doi.org/https://doi.org/10.1002/asia.201301334.

[30] Yesilgul N, Seven O, Guliyev R, Akkaya EU. Energy Harvesting in a Bodipy-Functionalized Rotaxane. J Org Chem 2018;83:13228–32. https://doi.org/10.1021/acs.joc.8b01928.

[31] Harriman A, Mallon LJ, Elliot KJ, Haefele A, Ulrich G, Ziessel R. Length Dependence for Intramolecular Energy Transfer in Three- and Four-Color

Donor−Spacer−Acceptor Arrays. J Am Chem Soc 2009;131:13375–86. https://doi.org/10.1021/ja9038856.

[32] Diring S, Puntoriero F, Nastasi F, Campagna S, Ziessel R. Star-Shaped Multichromophoric Arrays from Bodipy Dyes Grafted on Truxene Core. J Am Chem Soc 2009;131:6108–10. https://doi.org/10.1021/ja9015364.

[33] Patalag LJ, Hoche J, Mitric R, Werz DB, Feringa BL. Transforming Dyes into Fluorophores: Exciton-Induced Emission with Chain-like Oligo-BODIPY Superstructures. Angew Chem Int Ed 2022;61:e202116834. https://doi.org/https://doi.org/10.1002/anie.202116834.

[34] Ziessel R, Ulrich G, Olivier JH, Bura T, Sutter A. Carborane-Bodipy scaffolds for through space energy transfer. Chem Commun 2010;46:7978–80. https://doi.org/10.1039/C0CC02656E.

[35] Kong L, Wong HL, Tam AYY, Lam WH, Wu L, Yam VWW. Synthesis, Characterization, and Photophysical Properties of Bodipy-Spirooxazine and -Spiropyran Conjugates: Modulation of Fluorescence Resonance Energy Transfer Behavior via Acidochromic and Photochromic Switching. ACS Appl Mater Interfaces 2014;6:1550–62. https://doi.org/10.1021/am404242a.

[36] García-Rodríguez A, Porcu P, Estrada-Montaño AS, Vonlanthen M, Martínez-Serrano RD, Zaragoza-Galán G, Rivera E. Design of novel conjugated systems bearing donor-acceptor groups (pyrene-bodipy): Optical, photophysical properties and energy transfer. Dyes and Pigments 2021;185:108925. https://doi.org/10.1016/J.DYEPIG.2020.108925.

[37] Zou Y, Long S, Xiong T, Zhao X, Sun W, Du J, Fan J, Peng X. Single-Molecule Förster Resonance Energy Transfer-Based Photosensitizer for Synergistic Photodynamic/Photothermal Therapy. ACS Cent Sci 2021;7:327–34. https://doi.org/10.1021/acscentsci.0c01551.

[38] Fakis M, Beckwith JS, Seintis K, Martinou E, Nançoz C, Karakostas N, Petsalakis I, Pistolis G, Vauthey E. Energy transfer and charge separation dynamics in photoexcited pyrene–bodipy molecular dyads. Phys Chem Chem Phys 2018;20:837–49. https://doi.org/10.1039/C7CP06914F.

[39] Carlotti B, Poddar M, Elisei F, Spalletti A, Misra R. Energy-Transfer and Charge-Transfer Dynamics in Highly Fluorescent Naphthalimide-BODIPY Dyads: Effect of BODIPY Orientation. J Phys Chem C 2019;123:24362–74. https://doi.org/10.1021/acs.jpcc.9b05851.

[40] Yang J, Cai F, Desbois N, Huang L, Gros CP, Bolze F, Fang Y, Wang S, Xu HJ. Synthesis, spectroscopic characterization, one and two-photon absorption properties and electrochemistry of π-expanded BODIPYs dyes. Dyes and Pigments 2020;175:108173. https://doi.org/10.1016/J.DYEPIG.2019.108173.

[41] Barros LWT, Cardoso TAS, Bihlmeier A, Wagner D, Kölmel DK, Hörner A, Bräse S, Brito-Cruz CH, Padilha LA. Two-photon absorption in a series of 2,6-disubstituted BODIPY dyes. Phys Chem Chem Phys 2017;19:21683–90. https://doi.org/10.1039/C6CP07849D.

[42] Tao J, Sun D, Sun L, Li Z, Fu B, Liu J, Zhang L, Wang S, Fang Y, Xu H. Tuning the photo-physical properties of BODIPY dyes: Effects of 1, 3, 5, 7- substitution on their optical and electrochemical behaviours. Dyes and Pigments 2019;168:166–74. https://doi.org/10.1016/J.DYEPIG.2019.04.054.

[43] Zheng Q, Xu G, Prasad PN. Conformationally Restricted Dipyrromethene Boron Difluoride (BODIPY) Dyes: Highly Fluorescent, Multicolored Probes for Cellular Imaging. Chem Eur J 2008;14:5812–9. https://doi.org/https://doi.org/10.1002/chem.200800309.

[44] Bartelmess J, Baldrighi M, Nardone V, Parisini E, Buck D, Echegoyen L, Giordani S. Synthesis and Characterization of Far-Red/NIR-Fluorescent

BODIPY Dyes, Solid-State Fluorescence, and Application as Fluorescent Tags Attached to Carbon Nano-onions. Chem Eur J 2015;21:9727–32. https://doi.org/https://doi.org/10.1002/chem.201500877.

[45] Sajjad MT, Manousiadis PP, Orofino C, Cortizo-Lacalle D, Kanibolotsky AL, Rajbhandari S, Amarasinghe D, Chun H, Faulkner G, O'Brien DC, Skabara PJ, Turnbull GA, Samuel IDW. Fluorescent Red-Emitting BODIPY Oligofluorene Star-Shaped Molecules as a Color Converter Material for Visible Light Communications. Adv Opt Mater 2015;3:536–40. https://doi.org/https://doi.org/10.1002/adom.201400424.

[46] Chiang LY, Padmawar PA, Canteenwala T, Tan L-S, He GS, Kannan R, Vaia R, Lin TC, Zheng Q, Prasad PN. Synthesis of C60-diphenylaminofluorene dyad with large 2PA cross-sections and efficient intramolecular two-photon energy transfer. Chem Commun 2002:1854–5. https://doi.org/10.1039/B202681C.

[47] Brousmiche DW, Serin JM, Fréchet JMJ, He GS, Lin TC, Chung SJ, Prasad PN. Fluorescence Resonance Energy Transfer in a Novel Two-Photon Absorbing System. J Am Chem Soc 2003;125:1448–9. https://doi.org/10.1021/ja0288688.

[48] Brousmiche DW, Serin JM, Fréchet JMJ, He GS, Lin TC, Chung SJ, Prasad PN, Kannan R, Tan LS. Fluorescence Resonance Energy Transfer in Novel Multiphoton Absorbing Dendritic Structures. J Phys Chem B 2004;108:8592–600. https://doi.org/10.1021/jp049948w.

[49] Adhikary R, Barnes CA, Petrich JW. Solvation Dynamics of the Fluorescent Probe PRODAN in Heterogeneous Environments: Contributions from the Locally Excited and Charge-Transferred States. J Phys Chem B 2009;113:11999–2004. https://doi.org/10.1021/jp905139n.

[50] Fonin AV, Silonov SA, Antifeeva IA, Stepanenko OV, Stepanenko OV, Fefilova AS, Povarova OI, Gavrilova AA, Kuznetsova IM, Turoverov KK. Photophysical

Properties of BADAN Revealed in the Study of GGBP Structural Transitions. Int J Mol Sci 2021;22. https://doi.org/10.3390/ijms222011113.

[51] Gaus K, Gratton E, Kable EPW, Jones AS, Gelissen I, Kritharides L, Jessup W. Visualizing lipid structure and raft domains in living cells with two-photon microscopy. Proc Natl Acad Sci 2003;100:15554–9. https://doi.org/10.1073/pnas.2534386100.

[52] Kim HM, Jung C, Kim BR, Jung SY, Hong JH, Ko YG, Lee KJ, Cho BR. Environment-Sensitive Two-Photon Probe for Intracellular Free Magnesium Ions in Live Tissue. Angew Chem Int Ed 2007;46:3460–3. https://doi.org/https://doi.org/10.1002/anie.200700169.

[53] Kim HM, Cho BR. Small-Molecule Two-Photon Probes for Bioimaging Applications. Chem Rev 2015;115:5014–55. https://doi.org/10.1021/cr5004425.

[54] González-Vera JA, Lv F, Escudero D, Orte A, Guo X, Hao E, Talavera-Rodriguez EM, Jiao L, Boens N, Ruedas-Rama MJ. Unusual spectroscopic and photophysical properties of solvatochromic BODIPY analogues of Prodan. Dyes and Pigments 2020;182:108510. https://doi.org/10.1016/J.DYEPIG.2020.108510.

[55] Chandra B, Subramaniam R, Mallik S, Srivastava DK. Formulation of photocleavable liposomes and the mechanism of their content release. Org Biomol Chem 2006;4:1730–40. https://doi.org/10.1039/B518359F.

[56] Turshatov A, Busko D, Avlasevich Y, Miteva T, Landfester K, Baluschev S. Synergetic Effect in Triplet–Triplet Annihilation Upconversion: Highly Efficient Multi-Chromophore Emitter. Chem Phys Chem 2012;13:3112–5. https://doi.org/https://doi.org/10.1002/cphc.201200306.

[57] Kubin RF, Fletcher AN. Fluorescence quantum yields of some rhodamine dyes. J Lumin 1982;27:455–62. https://doi.org/10.1016/0022-2313(82)90045-X.

[58] Melhuish WH. Quantum efficiencies of fluorescence of organic substances: Effect of solvent and concentration of the fluorescent solute. J Phys Chem 1961;65:229–35. https://doi.org/10.1021/j100820a009.

[59] Valeur B, Berberan-Santos MN. Molecular Fluorescence: Principles and Applications. 2nd ed. Wiley-VCH; 2012.

[60] Terenziani F, Katan C, Badaeva E, Tretiak S, Blanchard-Desce M. Enhanced Two-Photon Absorption of Organic Chromophores: Theoretical and Experimental Assessments. Adv Mater 2008;20:4641–78. https://doi.org/https://doi.org/10.1002/adma.200800402.

[61] Frisch MJ, Trucks GW, Schlegel HB, Robb MA, Cheeseman JR, Scalmani G, et al. Gaussian 09, revision C.01 2009.

[62] Tomasi J, Mennucci B, Cammi R. Quantum Mechanical Continuum Solvation Models. Chem Rev 2005;105:2999–3094. https://doi.org/10.1021/cr9904009.

[63] Moressi MB, Zón MA, Fernández H. Electrochemical oxidation of 6-propionyl-2-(N,N-dimethylamino)naphthalene (prodan) in acetonitrile on Pt electrodes: Reversible dimerization of prodan radical cations. Can J Chem 2002;80:1232–41. https://doi.org/10.1139/v02-112.

[64] Sartin MM, Camerel F, Ziessel R, Bard AJ. Electrogenerated Chemiluminescence of B8amide: A BODIPY-Based Molecule with Asymmetric ECL Transients. J Phys Chem C 2008;112:10833–41. https://doi.org/10.1021/jp8011848.

[65] Pospíšil P, Luxem KE, Ener M, Sýkora J, Kocábová J, Gray HB, Vlček A, Hof M. Fluorescence Quenching of (Dimethylamino)naphthalene Dyes Badan and Prodan by Tryptophan in Cytochromes P450 and Micelles. J Phys Chem B 2014;118:10085–91. https://doi.org/10.1021/jp504625d.

[66] Greenfield SR, Svec WA, Gosztola D, Wasielewski MR. Multistep Photochemical Charge Separation in Rod-like Molecules Based on Aromatic Imides and Diimides. J Am Chem Soc 1996;118:6767–77. https://doi.org/10.1021/ja9600789.

[67] Rehm D, Weller A. Kinetik und Mechanismus der Elektronübertragung bei der Fluoreszenzlöschung in Acetonitril. Berichte Der Bunsengesellschaft Für Physikalische Chemie 1969;73:834–9. https://doi.org/https://doi.org/10.1002/bbpc.19690730818.

[68] Speiser S. Photophysics and Mechanisms of Intramolecular Electronic Energy Transfer in Bichromophoric Molecular Systems: Solution and Supersonic Jet Studies. Chem Rev 1996;96:1953–76. https://doi.org/10.1021/cr941193+.

[69] Zheng Q, Xu G, Prasad PN. Conformationally Restricted Dipyrromethene Boron Difluoride (BODIPY) Dyes: Highly Fluorescent, Multicolored Probes for Cellular Imaging. Chem Eur J 2008;14:5812–9. https://doi.org/https://doi.org/10.1002/chem.200800309.

[70] Zhang X, Xiao Y, Qi J, Qu J, Kim B, Yue X, Belfield KD. Long-Wavelength, Photostable, Two-Photon Excitable BODIPY Fluorophores Readily Modifiable for Molecular Probes. J Org Chem 2013;78:9153–60. https://doi.org/10.1021/jo401379g.